

**Searches for Scalar Top and Scalar Bottom Quarks in
 e^+e^- Interactions at $161 \text{ GeV} \leq \sqrt{s} \leq 183 \text{ GeV}$**

The L3 Collaboration

Abstract

Searches for scalar top and scalar bottom quarks have been performed at center-of-mass energies between 161 GeV and 183 GeV using the L3 detector at LEP. No signal is observed. Model-independent limits on production cross sections are determined for the two decay channels $\tilde{t}_1 \rightarrow c\tilde{\chi}_1^0$ and $\tilde{b}_1 \rightarrow b\tilde{\chi}_1^0$. Within the framework of the Minimal Supersymmetric extension of the Standard Model mass limits are derived. For mass differences between \tilde{t}_1 and $\tilde{\chi}_1^0$ greater than 10 GeV a 95% C.L. limit of 81.5 GeV is set on the mass of the Supersymmetric partner of the left-handed top. A supersymmetric partner of the left-handed bottom with a mass below 80 GeV is excluded at 95% C.L. if the mass difference between \tilde{b}_1 and $\tilde{\chi}_1^0$ is greater than 20 GeV.

Submitted to *Phys. Lett. B*

1 Introduction

In the Minimal Supersymmetric extension of the Standard Model (MSSM) [1] for each helicity state Standard Model (SM) quark q there is a corresponding scalar SUSY partner $\tilde{q}_{L,R}$. Generally, the mixing between left \tilde{q}_L and right \tilde{q}_R eigenstates is proportional to the corresponding quark mass. The heavy top quark enhances $\tilde{t}_L - \tilde{t}_R$ mixing leading to a large splitting between the two mass eigenstates. This is usually expressed in terms of the mixing angle, θ_{LR} . The lighter scalar top quark

$$\tilde{t}_1 = \tilde{t}_L \cos \theta_{LR} + \tilde{t}_R \sin \theta_{LR} \quad (1)$$

can well be in the discovery range of LEP. Large ratio of the vacuum expectation values of the two Higgs fields, $\tan \beta \gtrsim 10$, results in a large $\tilde{b}_L - \tilde{b}_R$ mixing that may also lead to a light sbottom \tilde{b}_1 .

In the present analysis R-parity conservation is assumed which implies that SUSY particles are produced in pairs; the heavier sparticles decay into lighter ones and the Lightest Supersymmetric Particle (LSP) is stable. In the MSSM the most plausible LSP candidate is the weakly interacting lightest neutralino, $\tilde{\chi}_1^0$.

The squark production at LEP proceeds via the exchange of virtual bosons in s-channel. The production cross section is governed by two free parameters: the squark mass, $m_{\tilde{q}}$, and the mixing angle, θ_{LR} [2]. At $\cos \theta_{LR} \sim 0.57$ (0.39) the stop (sbottom) decouples from the Z and the cross section is minimal. It reaches the maximum at $\cos \theta_{LR}=1$ when \tilde{t}_1 is the weak eigenstate \tilde{t}_L .

The decay mode of the squark depends mainly on its mass and the masses of the decay products. At LEP energies the most important channels for the stop are: $\tilde{t}_1 \rightarrow c\tilde{\chi}_1^0$, $\tilde{t}_1 \rightarrow b\tilde{\chi}_1^+$, and $\tilde{t}_1 \rightarrow b\nu_{\ell}\tilde{\ell} / b\tilde{\nu}_{\ell}$, where $\tilde{\chi}_1^0$ and $\tilde{\chi}_1^+$ are the lightest neutralino and chargino, respectively, and $\tilde{\ell}$, $\tilde{\nu}_{\ell}$ are the supersymmetric partners of the charged lepton and neutrino. The scalar top analysis is performed assuming 100% branching ratio for the decay channel $\tilde{t}_1 \rightarrow c\tilde{\chi}_1^0$. For sbottom the most important decay mode $\tilde{b}_1 \rightarrow b\tilde{\chi}_1^0$ is investigated under the same assumption. Although the $\tilde{t}_1 \rightarrow b\tilde{\chi}_1^{\pm}$ decay channel is the dominant one when kinematically allowed, the current limits on chargino mass [3] preclude this decay to occur.

The stop decay $\tilde{t}_1 \rightarrow c\tilde{\chi}_1^0$ is a second order weak decay and the lifetime of the \tilde{t}_1 is larger than the typical hadronisation time of 10^{-23} s. Thus the scalar top first hadronises into a colourless meson or baryon and then decays. For the sbottom the situation depends on the gaugino-higgsino content of the neutralino: the hadronisation is preferred for a gaugino like neutralino. In the present analysis we follow this scenario. Though hadronisation does not change the final event topology, it does affect event multiplicity, jet properties and event shape.

Previous searches for stop and sbottom have been performed at LEP [4] and at the TEVATRON [5].

2 Data Samples and Simulation

The data used in the present analysis were collected in 1996 and 1997 at $\sqrt{s}=161$ GeV, 172 GeV and 183 GeV with integrated luminosities of 10.7 pb^{-1} , 10.1 pb^{-1} and 55.2 pb^{-1} , respectively. The description of the L3 detector and its performance can be found in Reference [6].

Monte Carlo (MC) samples of signal events are generated using a PYTHIA [7] based event generator and varying the stop (sbottom) mass from 45 GeV up to the kinematical limit and the $\tilde{\chi}_1^0$ mass from 1 GeV to $M_{\tilde{t}_1}-2$ GeV ($M_{\tilde{b}_1}-5$ GeV). About 2000 events are generated at each mass

point. The following MC programs are used to generate Standard Model background processes: PYTHIA for $e^+e^- \rightarrow q\bar{q}$, $e^+e^- \rightarrow \gamma Z/\gamma Z$ and $e^+e^- \rightarrow Ze^+e^-$, KORALZ [8] for $e^+e^- \rightarrow \tau^+\tau^-$, KORALW [9] for $e^+e^- \rightarrow W^+W^-$, EXCALIBUR [10] for $e^+e^- \rightarrow W^\pm e^\mp \nu$, PHOJET [11] for $e^+e^- \rightarrow e^+e^-q\bar{q}$ and DIAG36 [12] for $e^+e^- \rightarrow e^+e^-\tau^+\tau^-$. The number of simulated events for each background process exceeds 100 times the statistics of the collected data samples except for the process $e^+e^- \rightarrow e^+e^-q\bar{q}$, for which three times more MC events are generated.

The detector response is simulated using the GEANT 3.15 package [13]. It takes into account effects of energy loss, multiple scattering and showering in the detector materials and in the beam pipe. Hadronic interactions are simulated with the GEISHA program [14].

3 Event Preselection

The signal events, $\tilde{t}_1 \rightarrow c\tilde{\chi}_1^0$ and $\tilde{b}_1 \rightarrow b\tilde{\chi}_1^0$, are characterised by two high multiplicity acoplanar jets containing c- or b-quarks. The two neutralinos in the final state escape the detector leading to missing energy in the event. A common preselection was applied to obtain a sample of unbalanced hadronic events and to reduce the background from two-photon interactions and from dilepton production. The events have to fulfil the following requirements: more than 4 tracks; at least 10 but not more than 40 calorimetric clusters; event visible energy, E_{vis} , larger than 3 GeV; an energy deposition in the forward calorimeters less than 10 GeV and a total energy in the 30° cone around the beam pipe less than $0.25 \times E_{vis}$; a missing momentum greater than 1 GeV.

After the preselection 900, 925 and 4378 data events are retained in the 161, 172 and 183 GeV data samples, respectively. This is to be compared with 1175, 1088 and 4217 events expected from the SM processes. The dominant contribution comes from two-photon interactions in which we observe a 10-20% normalisation uncertainty. Figure 1 shows the distributions of some kinematical variables for the data sample, the SM background expectations and the signal events at $\sqrt{s}=183$ GeV after preselection. The distributions of the event b-tagging variable D_{btag} and a b-tagging Neural Network output for a jet NN_{bjet} are shown in Figure 2. D_{btag} is defined as the negative log-likelihood of the probability for the event being consistent with light quark production. After preselection the data and MC are in a fair agreement.

4 Selection Optimisation

The kinematics of the signal events depends strongly on the mass difference between the squark and the neutralino, $\Delta M = M_{\tilde{q}} - M_{\tilde{\chi}_1^0}$. In the low ΔM region, between 5 and 10 GeV, visible energy and track multiplicity are low. Therefore the signal events are difficult to separate from the two-photon interactions. For high ΔM values, between 50 and 70 GeV, large visible energy and high track multiplicity cause the signal events to be similar to WW , $We\nu$ or ZZ final states. The most favourable region for the signal and background separation appears at $\Delta M=20-40$ GeV.

Searches are performed independently in different ΔM regions. At $\sqrt{s}=161$ GeV and 172 GeV three different selections have been designed for three ΔM regions, whereas for $\sqrt{s}=183$ GeV four selections have been optimised to account for the wider kinematical range. The most discriminating sets of cuts are obtained using an optimisation procedure which min-

imises the following sensitivity function [15]:

$$k = \sum_{i=0}^{\infty} k_n P_B(n)/\epsilon. \quad (2)$$

Here k_n is the 95% C.L. upper limit for n observed events. It is calculated without subtraction of expected background B when optimising the cuts for ΔM region of 5-20 GeV, and with background subtraction for higher ΔM values (see Results section). $P_B(n)$ is the Poisson probability function of n observation with the mean value of B and ϵ is the signal selection efficiency [16].

The following kinematical variables are used in the selections: the visible energy E_{vis} , the visible mass, M_{vis} , and the sum of the two jets transverse momenta. These variables allow to discriminate between signal and two-photon background. A further reduction of this background is achieved by rejecting events with a pair of collinear tracks. To discriminate hadronic W and Z decays an upper cut on E_{vis} is applied. W^+W^- events where one W decays leptonically and $W^\pm e^\mp \nu$ events are suppressed by vetoing energetic isolated leptons. A cut on the normalised parallel missing momentum $E_{\parallel}^{\text{miss}}/E_{\text{vis}}$ removes most of the $q\bar{q}$ events. The remaining $q\bar{q}$ contribution can be suppressed by applying cuts on jet acollinearity and acoplanarity. A veto on the energy deposition in the 25° azimuthal sector around the missing momentum direction suppresses the $\tau^+\tau^-$ events. For sbottom selection we make use of b-quarks appearance in the final state and apply a cut on the event b-tagging variable D_{btag} . The exact cut values for each ΔM region are chosen by the optimisation procedure as described above.

The achieved signal selection efficiencies for stop (sbottom) range from 5% (20%) to 45% (50%) depending on ΔM . The efficiencies are lowest at low ΔM values. The b quark from $\tilde{b}_1 \rightarrow b\tilde{\chi}_1^0$ forms a long-lived hadron which decays at distances up to 3 mm from the interaction point. Use of this information in the discriminant variable D_{btag} results in higher efficiencies for the $\tilde{b}_1 \rightarrow b\tilde{\chi}_1^0$ channel compared to $\tilde{t}_1 \rightarrow c\tilde{\chi}_1^0$.

5 Statistical and Systematic Errors

The errors arising from signal MC event statistics vary from 3% to 8% for stop and from 3% to 7% for sbottom depending on selection efficiencies.

The main systematic errors on the signal selection efficiency arise from the uncertainties in the $\tilde{t}_1\tilde{t}_1$ ($\tilde{b}_1\tilde{b}_1$) production, stop-(sbottom)-hadron formation and the decay scheme. We have studied in detail the following sources of systematic errors:

- The mixing angle $\cos\theta_{\text{LR}}$ between the left and right eigenstates. The stop (sbottom) signals have been generated assuming $\cos\theta_{\text{LR}}=1$. However, as the coupling between \tilde{t}_1 (\tilde{b}_1) and Z depends on $\cos\theta_{\text{LR}}$, the initial state radiation spectrum is also mixing angle dependent. The maximal influence of this source has been evaluated by generating signal samples with the values of $\cos\theta_{\text{LR}}$ when stop (sbottom) decouples from Z . The largest uncertainty in the selection efficiency, 4% for stop and 6% for sbottom, is observed at low $\Delta M \sim 5$ -10 GeV. With increasing ΔM the selection efficiencies are less affected by this source of systematics. At $\Delta M \sim 70$ GeV the error is estimated to be negligible.
- The Fermi motion parameter of the spectator quark(s) in the \tilde{t}_1 -(\tilde{b}_1)-hadron. The invariant mass available for spectator quark(s) has been assumed to be $M_{\text{eff}}=0.5$ GeV [17]. The hadronic energy and track multiplicity of the event depend on the value of this variable so

that a variation of M_{eff} from 0.25 GeV to 0.75 GeV [17] results in 4-12% relative change in efficiency for stop and 6-8% for sbottom.

- The Peterson fragmentation function parameter ϵ_b . For the \tilde{t}_1 -(\tilde{b}_1 -)hadron the Peterson fragmentation scheme [18] was used with $\epsilon_t(\epsilon_{\tilde{b}})$ propagated from ϵ_b so that $\epsilon_{\tilde{q}} = \epsilon_b m_b^2 / m_{\tilde{q}}^2$, $\epsilon_b = 0.0035$ [19] and $m_b = 5$ GeV. The ϵ_b was varied in the range from 0.002 to 0.006 [19]. This induces a 5-12% and 2-6% systematic effect in selection efficiencies for stop and sbottom, respectively.
- For the $\tilde{t}_1 \rightarrow c\tilde{\chi}_1^0$ decays the uncertainty on the c-quark fragmentation parameter ϵ_c results in a 1-4% change in efficiency when ϵ_c is varied from 0.02 to 0.06 [19]. The central value is chosen to be $\epsilon_c = 0.03$ [19].

For the $\tilde{t}_1 \rightarrow c\tilde{\chi}_1^0$ channel all sources of systematics have larger impact on lower ΔM selections. This is because the energy available for c-quarks is low and the variation of the $\cos\theta_{\text{LR}}$, M_{eff} , ϵ_b and ϵ_c has a relatively high influence on the event kinematics. In contrast, for the $\tilde{b}_1 \rightarrow b\tilde{\chi}_1^0$ decays, the systematic errors, except the one related to $\cos\theta_{\text{LR}}$, increase with increasing ΔM . This is because the sbottom selection relies strongly on the b-tagging at high ΔM , whereas at low values of ΔM the b-tagging is not applied. The \tilde{b}_1 hadronisation and decay scheme, especially the uncertainty on ϵ_b , have a noticeable impact on the b-jet track multiplicity and hardness, and consequently on the signal efficiency for the D_{btag} cut.

The overall systematic error ranges from 7% to 18% for stop. The $\Delta M \sim 5$ -10 GeV is the region of highest systematic uncertainty of about 15-18%. Above $\Delta M \sim 10$ -20 GeV the error decreases to 7%. For sbottom the highest overall uncertainty of about 10-12% is observed at very low, ~ 5 -10 GeV, and high, $\gtrsim 60$ GeV ΔM regions. In the intermediate ΔM region the systematic error amounts to 7-10%. The summary on statistical and systematic errors for $\tilde{t}_1 \rightarrow c\tilde{\chi}_1^0$ and $\tilde{b}_1 \rightarrow b\tilde{\chi}_1^0$ channels is given in Table 1 for 183 GeV. Similar numbers are found also at 161 and 172 GeV. In the final results the systematic error is incorporated using the method described in Reference [20].

6 Results

Table 2 summarises the number of selected data and expected background events for $\tilde{t}_1 \rightarrow c\tilde{\chi}_1^0$ and $\tilde{b}_1 \rightarrow b\tilde{\chi}_1^0$ channels. The contribution of two-fermion ($q\bar{q}$, $\tau^+\tau^-$), four-fermion (W^+W^- , $W^\pm e^\mp \nu$, ZZ , Ze^+e^-) and two-photon ($e^+e^-q\bar{q}$, $e^+e^-\tau^+\tau^-$) processes are given separately. No evidence for stop or sbottom was found and the upper limits on their production cross sections are derived. Due to the uncertainties in the simulation of two-photon interactions these contributions, conservatively, are not subtracted from data when deriving limits. The model-independent cross section limits for both scalar quarks in terms of $(M_{\tilde{q}}, M_{\tilde{\chi}_1^0})$ are given in Figure 3. No scaling of the production cross section has been applied when combining the 161 GeV, 172 GeV and 183 GeV analyses. Thus the evaluated limits correspond to luminosity weighted average cross section.

7 MSSM Interpretation

In MSSM the stop and sbottom production cross sections depend on the squark mass $M_{\tilde{q}}$ and the mixing angle $\cos\theta_{\text{LR}}$. The cross section is highest for the SUSY partner of left-handed

stop (sbottom), i.e. $\cos\theta_{LR}=1$, and has its minimum at $\cos\theta_{LR} \simeq 0.57$ (0.39). By comparing the theoretical prediction with the obtained 95% C.L. limit on production cross section we determine the excluded mass regions for \tilde{t}_1 and \tilde{b}_1 . Figure 4a) shows the excluded mass regions as a function of $M_{\tilde{q}}$ and $M_{\tilde{\chi}_1^0}$ for stop at $\cos\theta_{LR}=1$ and 0.57. The region excluded by the D0 experiment is also shown [5]. The corresponding exclusion plot for sbottom is given in Figure 4b) for $\cos\theta_{LR}=1$ and $\cos\theta_{LR}=0.39$. For a mass difference of $\Delta M = 15$ (35) GeV the excluded stop (sbottom) masses as a function of $\cos\theta_{LR}$ are shown in Figure 5.

Independent of $\cos\theta_{LR}$ the stop pair production is excluded at 95% C.L. for $M_{\tilde{t}_1}$ less than 72.5 GeV if the mass difference between stop and neutralino is larger than 10 GeV. For $\cos\theta_{LR} = 1$ and $\Delta M = 10$ GeV the exclusion limit is 81.5 GeV.

The sbottom production cross section at low $\cos\theta_{LR}$ is smaller, e.g. a factor of 4 at $\cos\theta_{LR}=0$, than that of the stop. Therefore for $\tilde{b}_1 \rightarrow b\tilde{\chi}_1^0$ channel, the exclusion limits are relatively low. A 95% C.L. lower limits for the sbottom mass are set at 80 GeV for ΔM greater than 20 GeV for $\cos\theta_{LR} = 1$ and 57 GeV for ΔM greater than 35 GeV with $\cos\theta_{LR} = 0.39$.

Acknowledgements

We wish to express our gratitude to the CERN accelerator division for the excellent performance of the LEP machine. We acknowledge the effort of all engineers and technicians who have participated in the construction and maintenance of this experiment. Special thanks go to our colleagues from the Institute of Theoretical Physics, Vienna University, A. Bartl and H. Eberl, and from the Vienna Institute of High Energy Physics, S. Kraml, W. Majerotto and W. Porod, for many useful discussions and comments.

The L3 Collaboration:

M. Acciarri,²⁸ O. Adriani,¹⁷ M. Aguilar-Benitez,²⁷ S. Ahlen,¹² J. Alcaraz,²⁷ G. Alemani,²³ J. Allaby,¹⁸ A. Aloisio,³⁰
 M.G. Alvigi,³⁰ G. Ambrosi,²⁰ H. Anderhub,⁴⁹ V.P. Andreev,^{7,38} T. Angelescu,¹⁴ F. Anselmo,¹⁰ A. Arefiev,²⁹ T. Azemoon,³
 T. Aziz,¹¹ P. Bagnaia,³⁷ L. Baksay,⁴⁴ S. Banerjee,¹¹ Sw. Banerjee,¹¹ K. Banicz,⁴⁶ A. Barczyk,^{49,47} R. Barillere,¹⁸
 L. Barone,³⁷ P. Bartalini,²³ A. Baschirotto,²⁸ M. Basile,¹⁰ R. Battiston,³⁴ A. Bay,²³ F. Becattini,¹⁷ U. Becker,¹⁶ F. Behner,⁴⁹
 J. Berdugo,²⁷ P. Berges,¹⁶ B. Bertucci,³⁴ B.L. Betev,⁴⁹ S. Bhattacharya,¹¹ M. Biasini,³⁴ A. Biland,⁴⁹ G.M. Bilei,³⁴
 J.J. Blaising,⁴ S.C. Blyth,³⁵ G.J. Bobbink,² R. Bock,¹ A. Böhm,¹ L. Boldizar,¹⁵ B. Borgia,^{18,37} D. Bourilkov,⁴⁹
 M. Bourquin,²⁰ S. Braccini,²⁰ J.G. Branson,⁴⁰ V. Brigljevic,⁴⁹ I.C. Brock,³⁵ A. Buffini,¹⁷ A. Buijs,⁴⁵ J.D. Burger,¹⁶
 W.J. Burger,³⁴ J. Busenitz,⁴⁴ A. Button,³ X.D. Cai,¹⁶ M. Campanelli,⁴⁹ M. Capell,¹⁶ G. Cara Romeo,¹⁰ G. Carlino,³⁰
 A.M. Cartacci,¹⁷ J. Casaus,²⁷ G. Castellini,¹⁷ F. Cavallari,³⁷ N. Cavallo,³⁰ C. Cecchi,²⁰ M. Cerrada,²⁷ F. Cesaroni,²⁴
 M. Chamizo,²⁷ Y.H. Chang,⁵¹ U.K. Chaturvedi,¹⁹ M. Chemarin,²⁶ A. Chen,⁵¹ G. Chen,⁸ G.M. Chen,⁸ H.F. Chen,²¹
 H.S. Chen,⁸ X. Chereau,⁴ G. Chiefari,³⁰ C.Y. Chien,⁵ L. Cifarelli,³⁹ F. Cindolo,¹⁰ C. Civinini,¹⁷ I. Clare,¹⁶ R. Clare,¹⁶
 G. Coignet,⁴ A.P. Colijn,² N. Colino,²⁷ S. Costantini,⁹ F. Cotoroba,¹⁴ B. de la Cruz,²⁷ A. Csilling,¹⁵ T.S. Dai,¹⁶
 R.D' Alessandro,¹⁷ R. de Asmundis,³⁰ A. Degré,⁴ K. Deiters,⁴⁷ D. della Volpe,³⁰ P. Denes,³⁶ F. DeNotaristefani,³⁷
 M. Diemoz,³⁷ D. van Dierendonck,² F. Di Lodovico,⁴⁹ C. Dionisi,^{18,37} M. Dittmar,⁴⁹ A. Dominguez,⁴⁰ A. Doria,³⁰
 M.T. Dova,^{9,‡} D. Duchesneau,⁴ P. Duinker,² I. Duran,⁴¹ S. Easo,³⁴ H. El Mamouni,²⁶ A. Engler,³⁵ F.J. Eppling,¹⁶
 F.C. Erné,² P. Extermann,²⁰ M. Fabre,⁴⁷ R. Faccini,³⁷ M.A. Falagan,²⁷ S. Falciano,³⁷ A. Favara,¹⁷ J. Fay,²⁶ O. Fedin,³⁸
 M. Felcini,⁴⁹ T. Ferguson,³⁵ F. Ferroni,³⁷ H. Fesefeldt,¹ E. Fiandrini,³⁴ J.H. Field,²⁰ F. Filthaut,¹⁸ P.H. Fisher,¹⁶ I. Fisk,⁴⁰
 G. Forconi,¹⁶ L. Fredj,²⁰ K. Freudenreich,⁴⁹ C. Furetta,²⁸ Yu. Galaktionov,^{29,16} S.N. Ganguli,¹¹ P. Garcia-Abia,⁶
 M. Gataullin,³³ S.S. Gau,¹³ S. Gentile,³⁷ N. Gheordanescu,¹⁴ S. Giagu,³⁷ S. Goldfarb,²³ J. Goldstein,¹² Z.F. Gong,²¹
 A. Gougas,⁵ G. Gratta,³³ M.W. Gruenewald,⁹ R. van Gulik,² V.K. Gupta,³⁶ A. Gurtu,¹¹ L.J. Gutay,⁴⁶ D. Haas,⁶
 B. Hartmann,¹ A. Hasan,³¹ D. Hatzifotiadou,¹⁰ T. Hebbeker,⁹ A. Hervé,¹⁸ P. Hidas,¹⁵ J. Hirschfelder,³⁵ W.C. van Hoek,³²
 H. Hofer,⁴⁹ H. Hoorani,³⁵ S.R. Hou,⁵¹ G. Hu,⁵ I. Iashvili,⁴⁸ B.N. Jin,⁸ L.W. Jones,³ P. de Jong,¹⁸ I. Josa-Mutuberria,²⁷
 R.A. Khan,¹⁹ D. Kamrad,⁴⁸ J.S. Kapustinsky,²⁵ M. Kaur,^{19,‡} M.N. Kienzle-Focacci,²⁰ D. Kim,¹⁷ D.H. Kim,⁴³ J.K. Kim,⁴³
 S.C. Kim,⁴³ W.W. Kinnison,²⁵ A. Kirkby,³³ D. Kirkby,³³ J. Kirkby,¹⁸ D. Kiss,¹⁵ W. Kittel,³² A. Klimentov,^{16,29}
 A.C. König,³² A. Kopp,⁴⁸ I. Korolko,²⁹ V. Koutsenko,^{16,29} R.W. Kraemer,³⁵ W. Krenz,¹ A. Kunin,^{16,29} P. Lacentre,^{48,‡,‡}
 P. Ladron de Guevara,²⁷ I. Laktineh,²⁶ G. Landi,¹⁷ C. Lapointe,¹⁶ K. Lassila-Perini,⁴⁹ P. Laurikainen,²² A. Lavorato,³⁹
 M. Lebeau,¹⁸ A. Lebedev,¹⁶ P. Lebrun,²⁶ P. Lecomte,⁴⁹ P. Lecoq,¹⁸ P. Le Coultre,⁴⁹ H.J. Lee,⁹ J.M. Le Goff,¹⁸ R. Leiste,⁴⁸
 E. Leonardi,³⁷ P. Levchenko,³⁸ C.Li,²¹ C.H. Lin,⁵¹ W.T. Lin,⁵¹ F.L. Linde,^{2,18} L. Lista,³⁰ Z.A. Liu,⁸ W. Lohmann,⁴⁸
 E. Longo,³⁷ W. Lu,³³ Y.S. Lu,⁸ K. Lübelmeyer,¹ C. Luci,^{18,37} D. Luckey,¹⁶ L. Luminari,³⁷ W. Lustermaan,⁴⁹ W.G. Ma,²¹
 M. Maity,¹¹ G. Majumder,¹¹ L. Malgeri,¹⁸ A. Malinin,²⁹ C. Mañá,²⁷ D. Mangeol,³² P. Marchesini,⁴⁹ G. Marian,^{44,‡}
 A. Marin,¹² J.P. Martin,²⁶ F. Marzano,³⁷ G.G.G. Massaro,²⁰ K. Mazumdar,¹¹ R.R. McNeil,⁷ S. Mele,¹⁸ L. Merola,³⁰
 M. Meschini,¹⁷ W.J. Metzger,³² M. von der Mey,¹ D. Miganj,¹⁰ A. Mihul,¹⁴ A.J.W. van Mil,³² H. Milcent,¹⁸ G. Mirabelli,³⁷
 J. Mnich,¹⁸ P. Molnar,⁹ B. Monteleoni,¹⁷ R. Moore,³ T. Moulík,¹¹ R. Mount,³³ G.S. Muanza,²⁶ F. Muheim,²⁰ A.J.M. Muijs,²
 S. Nahn,¹⁶ M. Napolitano,³⁰ F. Nessi-Tedaldi,⁴⁹ H. Newman,³³ T. Niessen,¹ A. Nippe,²³ A. Nisati,³⁷ H. Nowak,⁴⁸ Y.D. Oh,⁴³
 G. Organtini,³⁷ R. Ostonen,²² C. Palomares,²⁷ D. Pandoulas,¹ S. Paoletti,^{37,18} P. Paolucci,³⁰ H.K. Park,³⁵ I.H. Park,⁴³
 G. Pascale,³⁷ G. Passaleva,¹⁸ S. Patricelli,³⁰ T. Paul,¹³ M. Pauluzzi,³⁴ C. Paus,¹⁸ F. Pauss,⁴⁹ D. Peach,¹⁸ M. Pedace,³⁷
 Y.J. Pei,¹ S. Pensotti,²⁸ D. Perret-Gallix,⁴ B. Petersen,³² S. Petrak,⁹ A. Pevsner,⁵ D. Piccolo,³⁰ M. Pieri,¹⁷ P.A. Piroué,³⁶
 E. Pistolessi,²⁸ V. Plyaskin,²⁹ M. Pohl,⁴⁹ V. Pojidaev,^{29,17} H. Postema,¹⁶ J. Pothier,¹⁸ N. Produit,²⁰ D. Prokofiev,³⁸
 J. Quartieri,³⁹ G. Rahal-Callot,⁴⁹ N. Raja,¹¹ P.G. Rancoita,²⁸ M. Rattaggi,²⁸ G. Raven,⁴⁰ P. Razis,³¹ D. Ren,⁴⁹
 M. Rescigno,³⁷ S. Reucroft,¹³ T. van Rhee,⁴⁵ S. Riemann,⁴⁸ K. Riles,³ A. Robohm,⁴⁹ J. Rodin,⁴⁴ B.P. Roe,³ L. Romero,²⁷
 S. Rosier-Lees,⁴ S. Roth,¹ J.A. Rubio,¹⁸ D. Ruschmeier,⁹ H. Rykaczewski,⁴⁹ S. Sakar,³⁷ J. Salicio,¹⁸ E. Sanchez,²⁷
 M.P. Sanders,³² M.E. Sarakinos,²² C. Schäfer,¹ V. Schegelsky,³⁸ S. Schmidt-Kaerst,¹ D. Schmitz,¹ N. Scholz,⁴⁹
 H. Schopper,⁵⁰ D.J. Schotanus,³² J. Schwenke,¹ G. Schwering,¹ C. Sciacca,³⁰ D. Sciarino,²⁰ L. Servoli,³⁴ S. Shevchenko,³³
 N. Shivarov,⁴² V. Shoutko,²⁹ J. Shukla,²⁵ E. Shumilov,²⁹ A. Shvorob,³³ T. Siedenburger,¹ D. Son,⁴³ B. Smith,¹⁶
 P. Spillantini,¹⁷ M. Steuer,¹⁶ D.P. Stickland,³⁶ A. Stone,⁷ H. Stone,³⁶ B. Stoyanov,⁴² A. Straessner,¹ K. Sudhakar,¹¹
 G. Sultanov,¹⁹ L.Z. Sun,²¹ G.F. Susinno,²⁰ H. Suter,⁴⁹ J.D. Swain,¹⁹ X.W. Tang,⁸ L. Tauscher,⁶ L. Taylor,¹³
 C. Timmermans,³² Samuel C.C. Ting,¹⁶ S.M. Ting,¹⁶ S.C. Tonwar,¹¹ J. Tóth,¹⁵ C. Tully,³⁶ K.L. Tung,⁸ Y. Uchida,¹⁶
 J. Ulbricht,⁴⁹ E. Valente,³⁷ G. Vesztegombi,¹⁵ I. Vetlitsky,²⁹ G. Viertel,⁴⁹ S. Villa,¹³ M. Vivargent,⁴ S. Vlachos,⁶ H. Vogel,³⁵
 H. Vogt,⁴⁸ I. Vorobiev,^{18,29} A.A. Vorobyov,³⁸ A. Vorvolakos,³¹ M. Wadhwa,⁶ W. Wallraff,¹ J.C. Wang,¹⁶ X.L. Wang,²¹
 Z.M. Wang,²¹ A. Weber,¹ S.X. Wu,¹⁶ S. Wynhoff,¹ J. Xu,¹² Z.Z. Xu,²¹ B.Z. Yang,²¹ C.G. Yang,⁸ H.J. Yang,⁸ M. Yang,⁸
 J.B. Ye,²¹ S.C. Yeh,⁵² J.M. You,³⁵ An. Zalite,³⁸ Yu. Zalite,³⁸ P. Zemp,⁴⁹ Y. Zeng,¹ Z.P. Zhang,²¹ B. Zhou,¹² G.Y. Zhu,⁸
 R.Y. Zhu,³³ A. Zichichi,^{10,18,19} F. Ziegler,⁴⁸ G. Zilizi.^{44,‡}

- 1 I. Physikalisches Institut, RWTH, D-52056 Aachen, FRG[§]
III. Physikalisches Institut, RWTH, D-52056 Aachen, FRG[§]
 - 2 National Institute for High Energy Physics, NIKHEF, and University of Amsterdam, NL-1009 DB Amsterdam, The Netherlands
 - 3 University of Michigan, Ann Arbor, MI 48109, USA
 - 4 Laboratoire d'Annecy-le-Vieux de Physique des Particules, LAPP, IN2P3-CNRS, BP 110, F-74941 Annecy-le-Vieux CEDEX, France
 - 5 Johns Hopkins University, Baltimore, MD 21218, USA
 - 6 Institute of Physics, University of Basel, CH-4056 Basel, Switzerland
 - 7 Louisiana State University, Baton Rouge, LA 70803, USA
 - 8 Institute of High Energy Physics, IHEP, 100039 Beijing, China[△]
 - 9 Humboldt University, D-10099 Berlin, FRG[§]
 - 10 University of Bologna and INFN-Sezione di Bologna, I-40126 Bologna, Italy
 - 11 Tata Institute of Fundamental Research, Bombay 400 005, India
 - 12 Boston University, Boston, MA 02215, USA
 - 13 Northeastern University, Boston, MA 02115, USA
 - 14 Institute of Atomic Physics and University of Bucharest, R-76900 Bucharest, Romania
 - 15 Central Research Institute for Physics of the Hungarian Academy of Sciences, H-1525 Budapest 114, Hungary[‡]
 - 16 Massachusetts Institute of Technology, Cambridge, MA 02139, USA
 - 17 INFN Sezione di Firenze and University of Florence, I-50125 Florence, Italy
 - 18 European Laboratory for Particle Physics, CERN, CH-1211 Geneva 23, Switzerland
 - 19 World Laboratory, FBLJA Project, CH-1211 Geneva 23, Switzerland
 - 20 University of Geneva, CH-1211 Geneva 4, Switzerland
 - 21 Chinese University of Science and Technology, USTC, Hefei, Anhui 230 029, China[△]
 - 22 SEFT, Research Institute for High Energy Physics, P.O. Box 9, SF-00014 Helsinki, Finland
 - 23 University of Lausanne, CH-1015 Lausanne, Switzerland
 - 24 INFN-Sezione di Lecce and Università Degli Studi di Lecce, I-73100 Lecce, Italy
 - 25 Los Alamos National Laboratory, Los Alamos, NM 87544, USA
 - 26 Institut de Physique Nucléaire de Lyon, IN2P3-CNRS, Université Claude Bernard, F-69622 Villeurbanne, France
 - 27 Centro de Investigaciones Energeticas, Medioambientales y Tecnológicas, CIEMAT, E-28040 Madrid, Spain[‡]
 - 28 INFN-Sezione di Milano, I-20133 Milan, Italy
 - 29 Institute of Theoretical and Experimental Physics, ITEP, Moscow, Russia
 - 30 INFN-Sezione di Napoli and University of Naples, I-80125 Naples, Italy
 - 31 Department of Natural Sciences, University of Cyprus, Nicosia, Cyprus
 - 32 University of Nijmegen and NIKHEF, NL-6525 ED Nijmegen, The Netherlands
 - 33 California Institute of Technology, Pasadena, CA 91125, USA
 - 34 INFN-Sezione di Perugia and Università Degli Studi di Perugia, I-06100 Perugia, Italy
 - 35 Carnegie Mellon University, Pittsburgh, PA 15213, USA
 - 36 Princeton University, Princeton, NJ 08544, USA
 - 37 INFN-Sezione di Roma and University of Rome, "La Sapienza", I-00185 Rome, Italy
 - 38 Nuclear Physics Institute, St. Petersburg, Russia
 - 39 University and INFN, Salerno, I-84100 Salerno, Italy
 - 40 University of California, San Diego, CA 92093, USA
 - 41 Dept. de Física de Partículas Elementales, Univ. de Santiago, E-15706 Santiago de Compostela, Spain
 - 42 Bulgarian Academy of Sciences, Central Lab. of Mechatronics and Instrumentation, BU-1113 Sofia, Bulgaria
 - 43 Center for High Energy Physics, Adv. Inst. of Sciences and Technology, 305-701 Taejeon, Republic of Korea
 - 44 University of Alabama, Tuscaloosa, AL 35486, USA
 - 45 Utrecht University and NIKHEF, NL-3584 CB Utrecht, The Netherlands
 - 46 Purdue University, West Lafayette, IN 47907, USA
 - 47 Paul Scherrer Institut, PSI, CH-5232 Villigen, Switzerland
 - 48 DESY-Institut für Hochenergiephysik, D-15738 Zeuthen, FRG
 - 49 Eidgenössische Technische Hochschule, ETH Zürich, CH-8093 Zürich, Switzerland
 - 50 University of Hamburg, D-22761 Hamburg, FRG
 - 51 National Central University, Chung-Li, Taiwan, China
 - 52 Department of Physics, National Tsing Hua University, Taiwan, China
- [§] Supported by the German Bundesministerium für Bildung, Wissenschaft, Forschung und Technologie
[‡] Supported by the Hungarian OTKA fund under contract numbers T019181, F023259 and T024011.
[¶] Also supported by the Hungarian OTKA fund under contract numbers T22238 and T026178.
[‡] Supported also by the Comisión Interministerial de Ciencia y Tecnología.
[‡] Also supported by CONICET and Universidad Nacional de La Plata, CC 67, 1900 La Plata, Argentina.
[‡] Supported by Deutscher Akademischer Austauschdienst.
[◇] Also supported by Panjab University, Chandigarh-160014, India.
[△] Supported by the National Natural Science Foundation of China.

References

- [1] For a review see, e.g. H.E. Haber and G.L. Kane, Phys. Rep. **117** (1985) 75.
- [2] A. Bartl *et al.*, Z.Phys **C 73** (1997) 469.
- [3] The L3 Collaboration, Search for Charginos and Neutralinos in e^+e^- Collisions at $\sqrt{s} = 161 - 183$ GeV, paper in preparation.
- [4] The ALEPH Collaboration, R. Barate *et al.*, Preprint CERN-EP/98-076, subm. to Phys. Lett. B; The DELPHI Collaboration, P. Abreu *et al.*, Phys.Lett. **B 387** (1996) 651; The OPAL Collaboration, K. Ackerstaff *et al.*, Preprint CERN-EP/98-107.
- [5] The D0 Collaboration, S. Abachi *et al.*, Phys. Rev. Lett. **76** (1996) 2222.
- [6] The L3 Collaboration, B. Adeva *et al.*, Nucl. Instr. and Meth. **A 289** (1990) 35; M. Chemarin *et al.*, Nucl. Instr. and Meth. **A 349** (1994) 345; M. Acciarri *et al.*, Nucl. Instr. and Meth. **A 351** (1994) 300; G. Basti *et al.*, Nucl. Instr. and Meth. **A 374** (1996) 293; I.C. Brock *et al.*, Nucl. Instr. and Meth. **A 381** (1996) 236; A. Adam *et al.*, Nucl. Instr. and Meth. **A 383** (1996) 342.
- [7] T. Sjöstrand, PYTHIA 5.7 and JETSET 7.4 Physics and Manual, CERN-TH/7112/93 (1993), revised August 1995; Comp. Phys. Comm. **82** (1994) 74.
- [8] S. Jardach, B.F.L. Ward, and Z. Wąs, Comp. Phys. Comm. **79** (1994) 503. Version 4.02 was used.
- [9] M. Skrzypek, S. Jardach, W. Placzek, and Z. Wąs, Comp. Phys. Comm. **94** (1996) 216; M. Skrzypek, S. Jardach, M. Martinez, W. Placzek, and Z. Wąs, Phys. Lett. **B 372** (1996) 289. Version 1.21 was used.
- [10] F.A. Berends, R.Kleiss, and R.Pittau, Nucl. Phys. **B 424** (1994) 308; Nucl. Phys. **B 426** (1994) 344; Nucl. Phys.(Proc. Suppl.) **B 37** (1994) 163; Phys. Lett. **B 335** (1994) 490; Comp.Phys.Comm. **83** (1994) 141.
- [11] R. Engel, Z. Phys. **C 66** (1995) 203; R. Engel and J. Ranft, Phys. Rev. **D 54** (1996) 4244. Version 1.05 was used.
- [12] F.A. Berends, P.H. Daverfeldt and R. Kleiss, Nucl. Phys. **B 253** (1985) 441.
- [13] R. Brun *et al.*, CERN DD/EE/84-1 (Revised 1987).
- [14] H. Fesefeldt, RWTH Aachen Report PITHA 85/2 (1985).
- [15] J.F. Grivaz and F. Le Diberder, preprint LAL-92-37, June 1992.
- [16] The L3 Collaboration, M. Acciarri *et al.*, E. Phys. J. **C 4** (1998) 207.
- [17] D.S. Hwang, C.S. Kim and W. Namgung, Preprint hep-ph/9412377; V. Barger, C.S. Kim and R.J.N. Phillips, Preprint MAD/PH/501, 1989.

- [18] C. Peterson *et al.*, Phys. Rev. **D 27** (1983) 105.
- [19] The LEP Experiments: ALEPH, DELPHI, L3, OPAL, Nucl. Instr. and Meth. **A 378** (1996) 101.
- [20] R.D. Cousins and V.L. Highland, Nucl. Inst. Meth. **A 320** (1992) 331.

Table 1: Relative statistical error on stop and sbottom selection efficiencies and contribution from various systematic uncertainties for 183 GeV. The lower part of the table shows the overall systematic error in different ΔM regions.

Source	$\frac{\Delta\epsilon}{\epsilon}(\tilde{t}_1 \rightarrow c\tilde{\chi}_1^0)$, %	$\frac{\Delta\epsilon}{\epsilon}(\tilde{b}_1 \rightarrow b\tilde{\chi}_1^0)$, %
Statistical error	3-8	3-7
Spectator Fermi motion	4-12	6-8
Uncertainty on ϵ_b	5-12	2-6
Uncertainty on ϵ_c	1-4	–
Mixing angle θ_{LR}	1-4	2-6
Overall systematic error		
$\Delta M = 5-10$ GeV	15-18	10-12
$\Delta M = 10-20$ GeV	7-15	7-10
$\Delta M = 20-60$ GeV	7	7-10
$\Delta M \geq 60$ GeV	7	10-12

Table 2: Number of observed events, N_{data} , and Standard Model background expectations, $N_{\text{MC}}^{\text{all}}$, for the stop and sbottom selections at $\sqrt{s}=161$ GeV, 172 GeV and 183 GeV. The contribution of two-fermion ($q\bar{q}$, $\tau^+\tau^-$), four-fermion (W^+W^- , $W^\pm e^\mp\nu$, ZZ , Ze^+e^-) and two-photon ($e^+e^-q\bar{q}$, $e^+e^-\tau^+\tau^-$) processes are given separately. The errors are due to MC statistics only.

Channel	N_{data}	$N_{\text{MC}}^{\text{two-fermion}}$	$N_{\text{MC}}^{\text{four-fermion}}$	$N_{\text{MC}}^{\text{two-photon}}$	$N_{\text{MC}}^{\text{all}}$
$\tilde{t}_1 \rightarrow c\tilde{\chi}_1^0$, $\sqrt{s} = 161 - 172$ GeV	2	0.035 ± 0.009	0.96 ± 0.04	0.26 ± 0.26	1.3 ± 0.3
$\tilde{t}_1 \rightarrow c\tilde{\chi}_1^0$, $\sqrt{s} = 183$ GeV	1	0.056 ± 0.056	2.37 ± 0.09	0.45 ± 0.45	2.9 ± 0.5
$\tilde{b}_1 \rightarrow b\tilde{\chi}_1^0$, $\sqrt{s} = 161 - 172$ GeV	1	0.45 ± 0.08	1.06 ± 0.04	1.3 ± 0.7	2.8 ± 0.7
$\tilde{b}_1 \rightarrow b\tilde{\chi}_1^0$, $\sqrt{s} = 183$ GeV	2	0.010 ± 0.007	1.7 ± 0.08	1.4 ± 0.8	3.1 ± 0.8

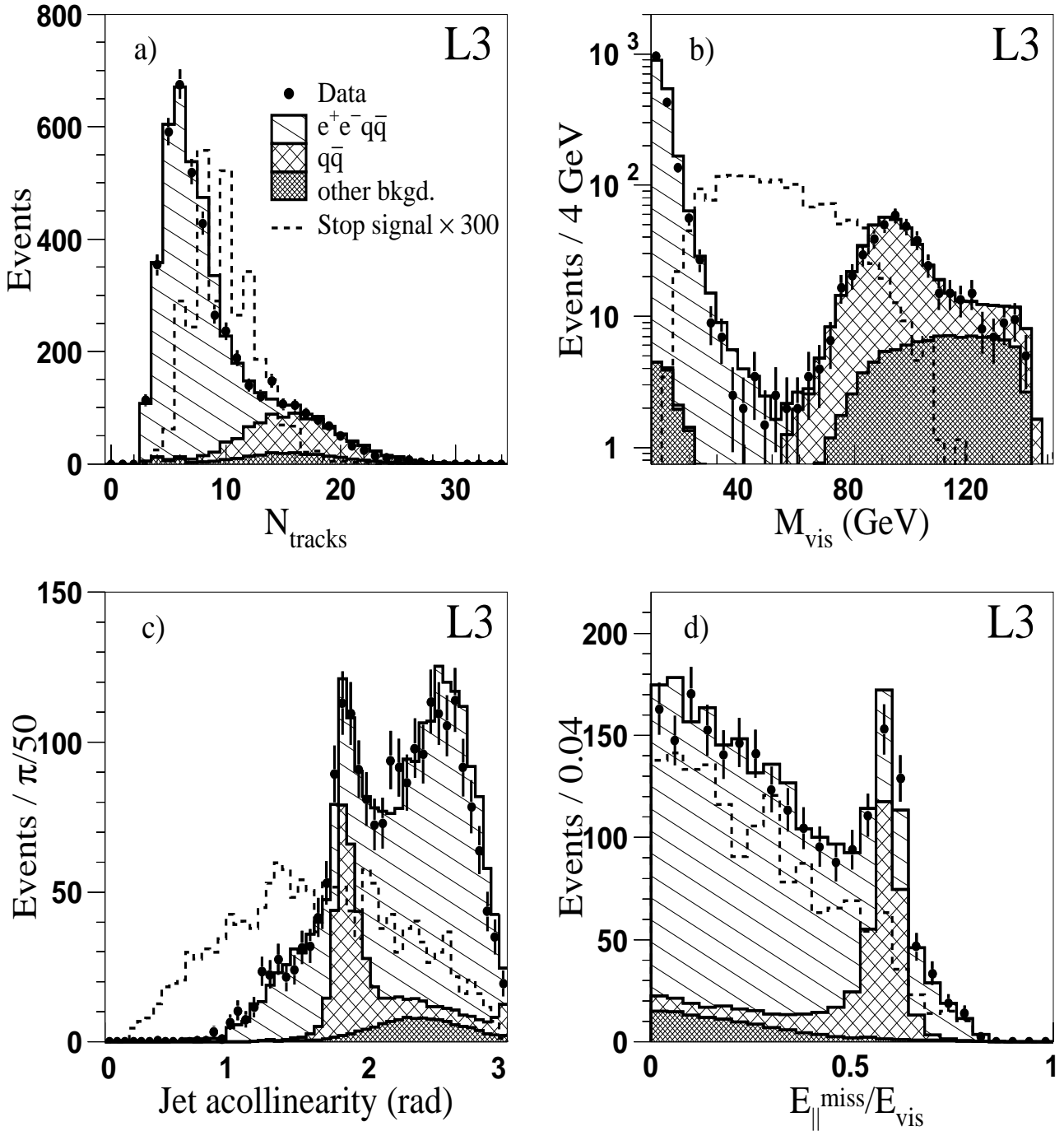


Figure 1: Distributions of a) track multiplicity, b) visible mass M_{vis} , c) jet acollinearity and d) normalised missing parallel energy $E_{\parallel}^{\text{miss}}/E_{\text{vis}}$ for data and Monte Carlo events at $\sqrt{s}=183$ GeV after preselection. Contributions from $e^+e^-q\bar{q}$, $q\bar{q}$ and other backgrounds, dominated by W^+W^- production, are given separately. For illustration the expected stop signal for $M_{\tilde{t}_1}=80$ GeV, $M_{\tilde{\chi}_1^0}=40$ GeV and $\cos\theta_{\text{LR}}=1$ is also shown.

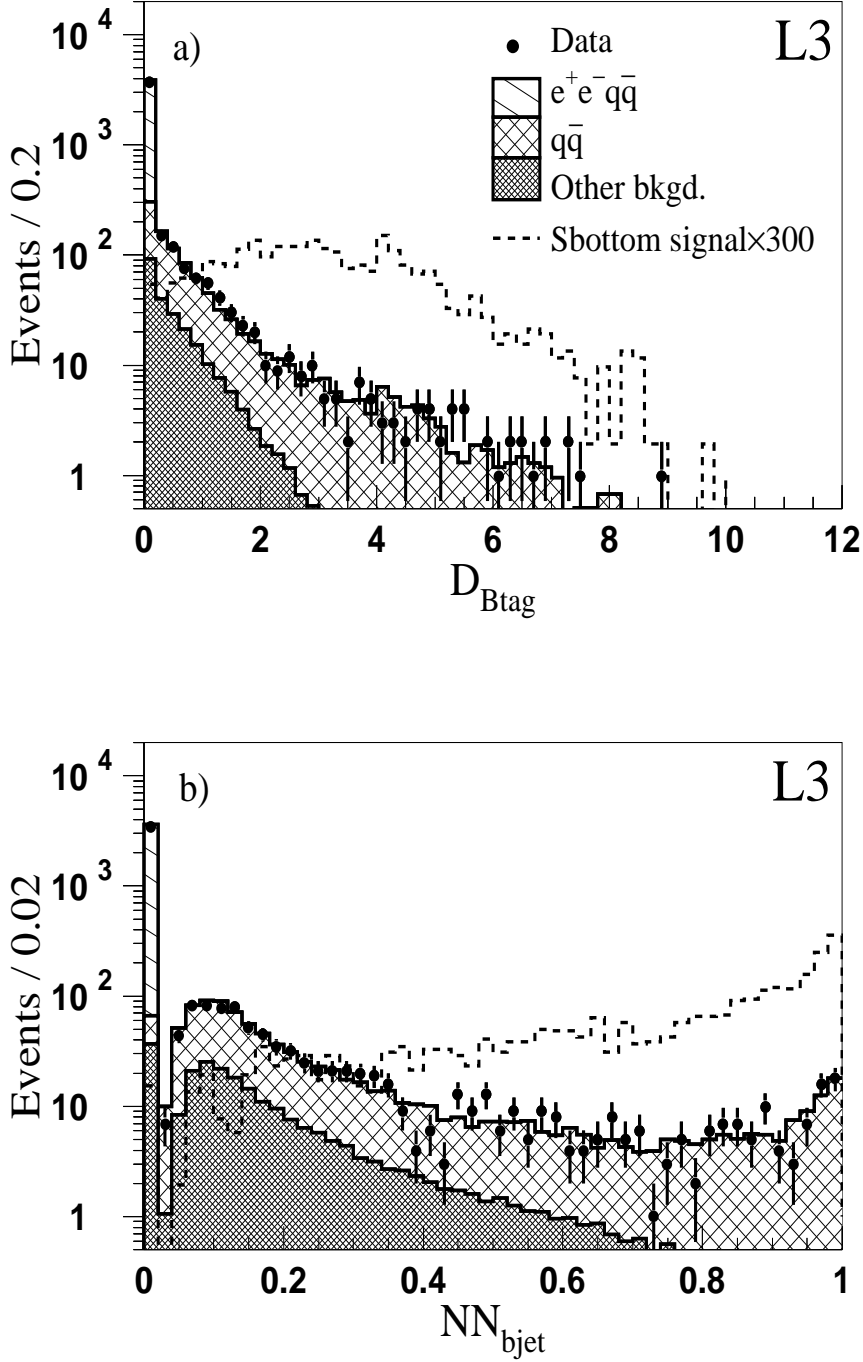


Figure 2: Distribution of a) the b-tagging event discriminant, defined as the negative log-likelihood of the probability for the event being consistent with light quark production, and b) b-tagging Neural Network output, NN_{bjet} , for data and Monte Carlo events at $\sqrt{s}=183$ GeV after preselection. Contributions from $e^+e^-q\bar{q}$, $q\bar{q}$ and other backgrounds, dominated by W^+W^- production, are given separately. For illustration the expected sbottom signal for $M_{\tilde{t}_1}=80$ GeV, $M_{\tilde{\chi}_1^0}=40$ GeV and $\cos\theta_{LR}=1$ is also shown.

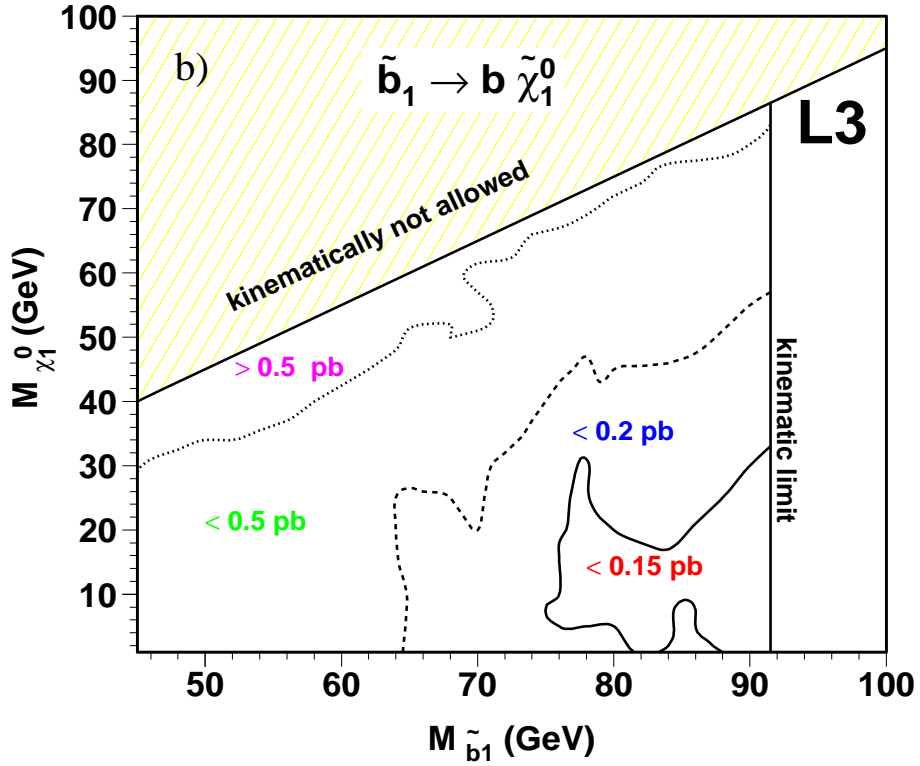
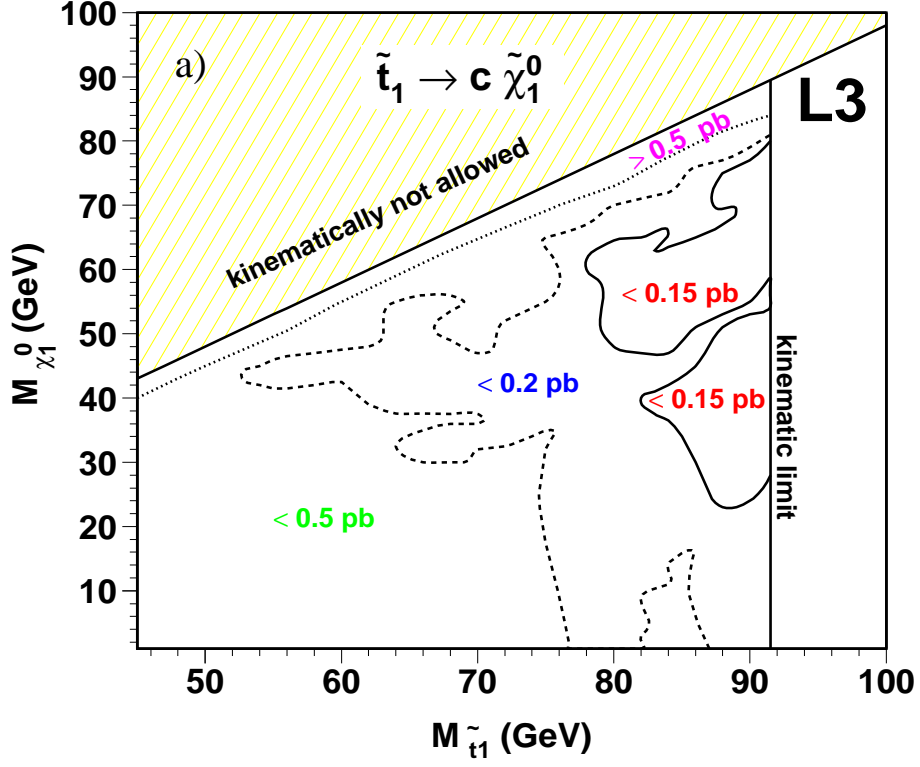


Figure 3: Upper limits on a) $e^+e^- \rightarrow \tilde{t}_1\tilde{t}_1$ and b) $e^+e^- \rightarrow \tilde{b}_1\tilde{b}_1$ production cross sections. In both cases the branching ratios are assumed to be 100%.

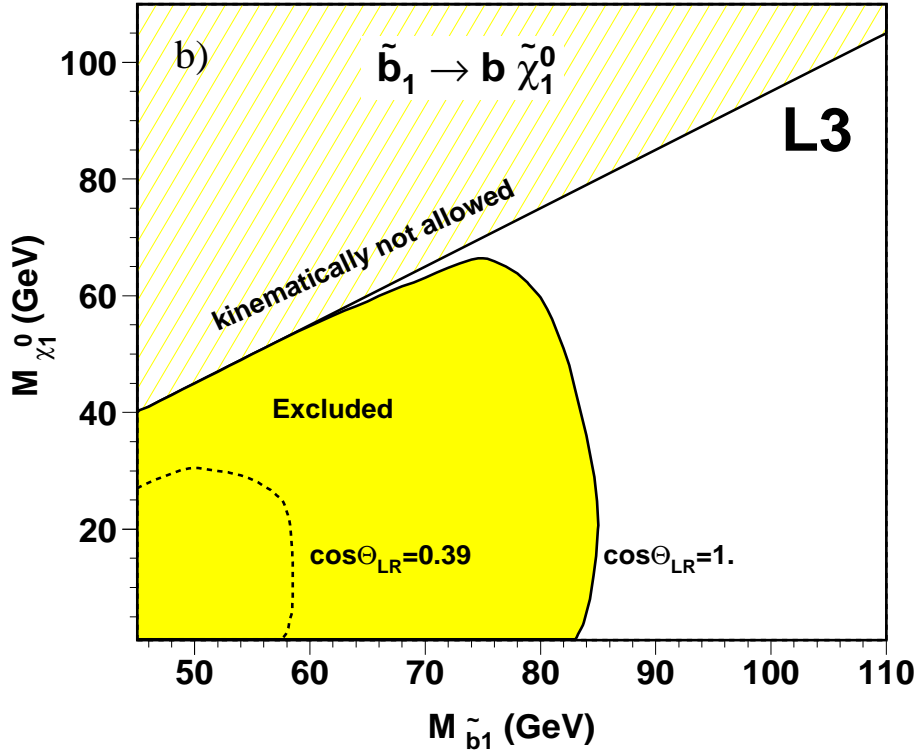
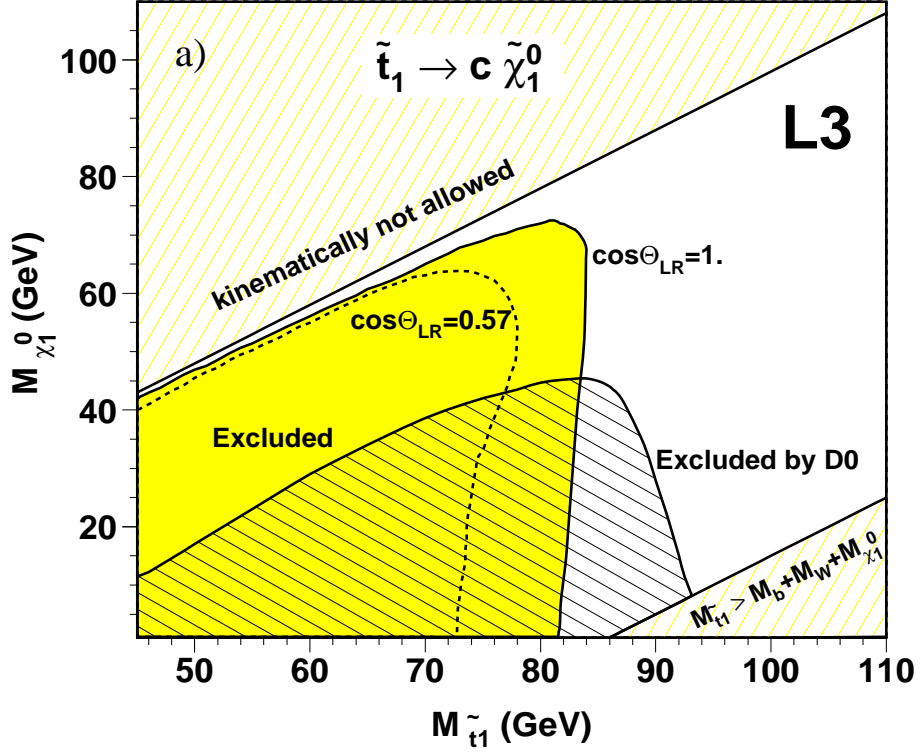


Figure 4: 95% C.L. exclusion limits for a) stop and b) sbottom as a function of the neutralino mass for maximal and minimal cross section assumptions. For comparison we show also result on stop searches from the D0 experiment.

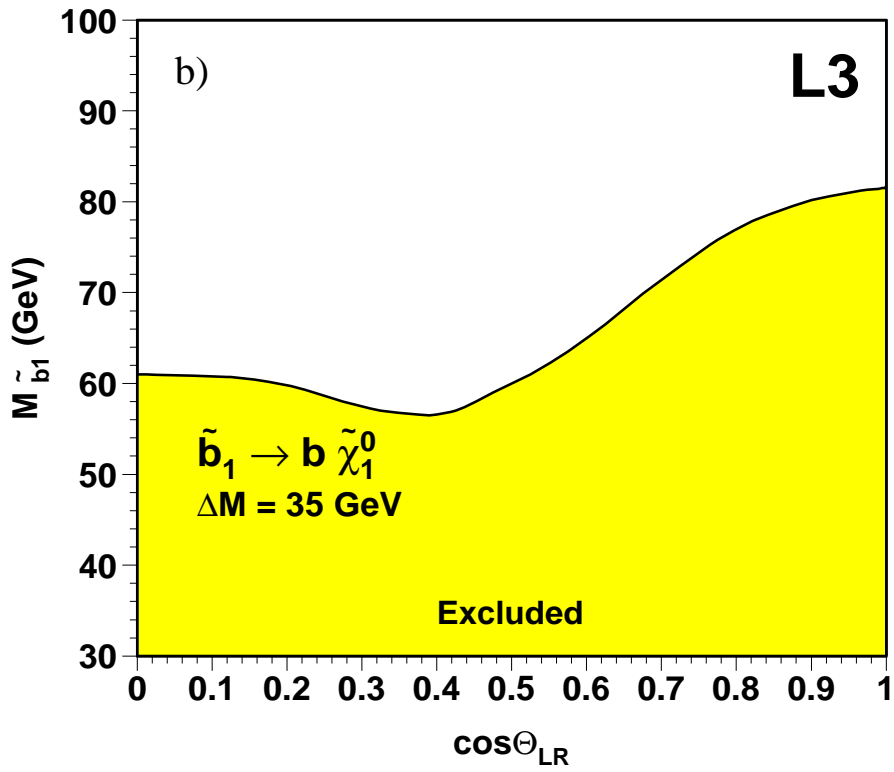
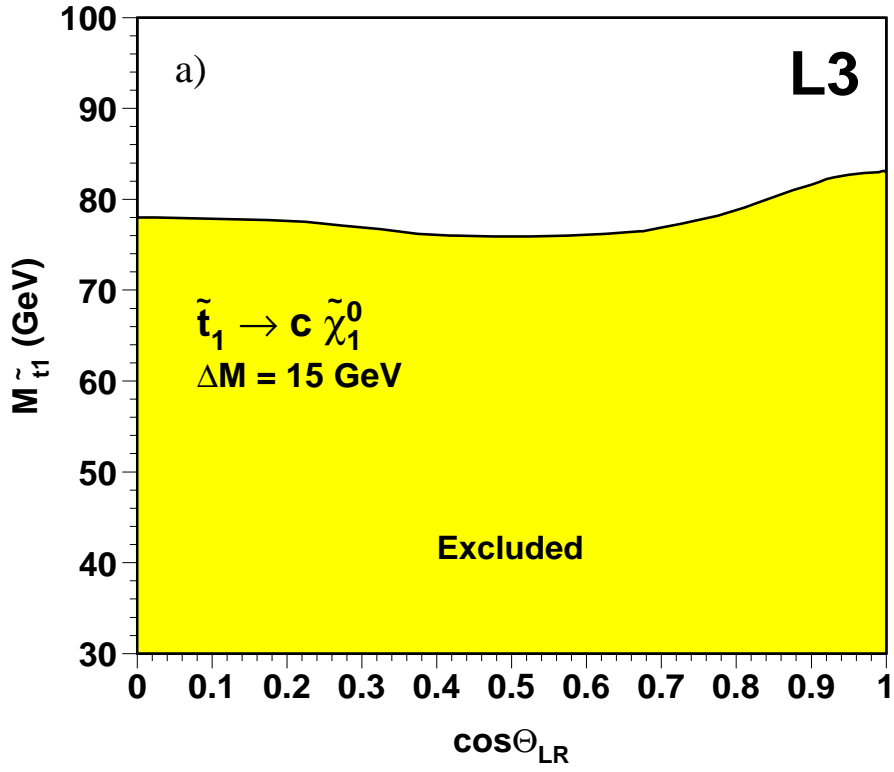


Figure 5: 95% C.L. exclusion limits for a) stop and b) sbottom masses as a function of $\cos\theta_{LR}$.